The elements of draping

E. Cerda[a,b,c], L. Mahadevan[a,c,d], and J. M. Pasini[b]

[a]Department of Applied Mathematics and Theoretical Physics, University of Cambridge, Wilberforce Road, Cambridge CB3 0WA, United Kingdom; and [b]Departmento de Física, Universidad de Santiago de Chile, Avenida Ecuador 3493, Casilla 307, Correo 2, Santiago, Chile

Communicated by John W. Hutchinson, Harvard University, Cambridge, MA, November 4, 2003 (received for review June 25, 2003)

We consider the gravity-induced draping of a 3D object with a naturally flat, isotropic elastic sheet. As the size of the sheet increases, we observe the appearance of new folded structures of increasing complexity that arise because of the competition between elasticity and gravity. We analyze some of the simpler 3D structures by determining their shape and analyzing their response and stability and show that these structures can easily switch between a number of metastable configurations. For more complex draperies, we derive scaling laws for the appearance and disappearance of new length scales. Our results are consistent with commonplace observations of drapes and complement large-scale computations of draping by providing benchmarks. They also yield a qualitative guide to fashion design and virtual reality animation.

The couturier drapes the 3D human body with a 2D fabric, working hard to subvert the relentless force of gravity to her cause by using a combination of cuts, folds, and tucks to transform a featureless textile into a piece of art. Indeed, the depiction of drapery, in the form of a carelessly thrown shawl on one's knee, is an important theme in Renaissance art, in both sculpture and sketching (1). Modern art has found another expression for the aesthetics of drapery in the carefully orchestrated wrapping of an entire building (2, 3). From a scientific viewpoint, drapery affords a common example of the complex patterns that arise from simple causes (Fig. 1*a*). In particular, drapery involves the large elastic (and reversible) deformations of naturally thin flat sheets,[e] a subject with comparatively recent theoretical origins going back to the early 20th century, when the first models valid for moderate deformations were formulated (4). In the last two or three decades, various geometrically exact formulations that go beyond the approximate theories have been put forward (5); these have also been the subject of large-scale computational approaches (6, 7). However, as is clearly evident in Fig. 1*a*, the fabric deformations in draping are highly inhomogeneous and result in the strong localization of strain in the neighborhood of points (8), thus making the computations difficult. Additionally, it is a matter of common experience that there are many local equilibria that the drapery is equally comfortable in; for example, the number of pleats in a skirt or sari can be easily modified to suit the wearer, suggesting a certain degeneracy among the solutions. To complement these quantitative computational approaches, which are in their nascent stages, here we approach the problem of drapery from a slightly different perspective by using a combination of exact analysis and scaling based on experimental observations of a variety of draping patterns to understand each of the above issues directly and thus provide a set of benchmarks while serving as a qualitative guide to the complexity of draping.

Visually dissecting the drape of a complex, relatively rigid surface, we see that it is constituted mostly of flat, cylindrical, and conical surfaces, which leave the body at a corner, along an edge, or along a curve (9). These elements of draping are clearly illustrated by considering three distinct but related examples: the suspension of a heavy elastic sheet from a point (Fig. 1*b*), along a straight line (Fig. 1*c*), or along a curved line (Fig. 1*d*).

Conical Folds and Euler's Elastica

To extract the main ingredients of the theory, we start by considering the "draping of a point" when a thin heavy circular sheet of thickness h and radius R, made of an isotropic material of density ρ, Young's modulus E, and Poisson ratio ν is suspended from its center. If the sheet is large, a conical shape with multiple flutes is observed (Fig. 1*b*). This latter structure is similar to the one studied earlier (8); however, here the number of folds is determined by the size of the sheet in proportion to the weight of the sheet. In such conical sheets, the Gauss curvature is localized to a small neighborhood of the tip, so that the stretching of the sheet can be neglected. More precisely this condition is met when the stretching strain is less than the bending strain. Since the sheet has a weight per unit length ρgRh, a typical stretching strain is $\rho gRh/Eh \sim \rho gR/E$. If the sheet is bent into a cylinder of radius, the typical strain caused by bending is h/R. The bending and stretching strain become comparable for a critical system size $R_s \sim (Eh/\rho g)^{1/2}$; when $R < R_s$ we can neglect the effects of stretching, whereas when $R > R_s$ we must account for stretching. For wrapping paper $R_s \approx 1$ m, whereas for rubber $R_s \approx 10$ cm. In this article, we will consider systems where we can neglect stretching everywhere so that $R \leq R_s$, although in reality even when $R > R_s$ stretching is important only in regions near the supporting points where the tension is largest.

A convenient coordinate system to describe a conical drape locates the origin at the vertex of the cone as shown in Fig. 2*b*. The vertical deflection is quantified by the z coordinate with $z > 0$ corresponding to the downward direction. The most general description of conical deformations uses the parametrization $\vec{r}(s, r) = r\mathbf{u}(s)$, where $\mathbf{u}$ is a unit vector characterized by an arc-length coordinate s, and r is the distance from the tip. Then the motion of $\mathbf{u}$ describes the curve $\mathcal{C}$ and the conical surface is conveniently defined in terms of the three Euler-like angles $[\theta(s), \beta(s), \phi(s)]$; the first two describe the unit vector $\mathbf{u}$, whereas the last describes the tangent to the curve $\mathcal{C}$. The inextensibility constraint dictates that the total length of this curve remains 2π and further that the coordinates (s, r) of a material point are an invariant of the deformation. Therefore, we may write

$$\begin{aligned} \mathbf{u}(s) &= \sin\beta\cos\theta\mathbf{e}_1 + \sin\beta\sin\theta\mathbf{e}_2 + \cos\beta\mathbf{e}_3 \\ &= \sin\beta\mathbf{e}_\rho + \cos\beta\mathbf{e}_3 \\ \mathbf{t}(s) &= \cos\phi\,\mathbf{e}_\theta + \sin\phi\,\mathbf{n}_\theta \\ \mathbf{n}(s) &= \sin\phi\,\mathbf{e}_\theta - \cos\phi\,\mathbf{n}_\theta, \end{aligned} \qquad [1]$$

where $\mathbf{e}_\rho$ is the radial unit vector in the horizontal plane, and $\mathbf{n}_\theta = \mathbf{u} \times \mathbf{e}_\theta$. Differentiating the first of the expressions in Eq. **1** and noting that $\mathbf{du}/\mathbf{ds} \equiv \dot{\mathbf{u}} = \mathbf{t}$, we get

$$\mathbf{t} = \cos\beta\dot{\beta}\mathbf{e}_\rho + \sin\beta\dot{\theta}\mathbf{e}_\theta - \dot{\beta}\sin\beta\mathbf{e}_3. \qquad [2]$$

[c]To whom correspondence should be addressed. E-mail: e.cerda@lauca.usach.cl or lm@deas.harvard.edu.

[d]Present address: Division of Engineering and Applied Sciences, Harvard University, 29 Oxford Street, Cambridge, MA 02138.

[e]Here and elsewhere, our view of large deformations corresponds to situations where the local strains in the sheet are small but the rotations of the cross section are large, so that the displacements can also be large.

www.pnas.org/cgi/doi/10.1073/pnas.0307160101

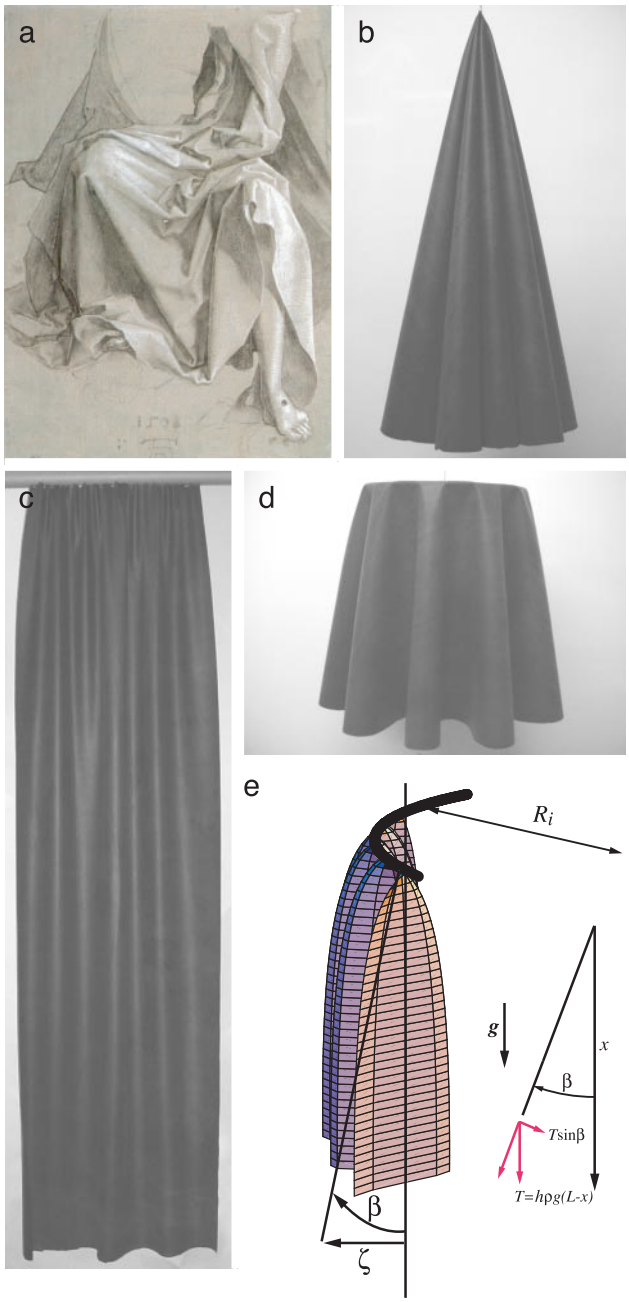

Fig. 1. Draping patterns. (*a*) Chiarascuro by Albrecht Durer (around *anno Domini* 1500). (*b–d*) Draping patterns induced by a sheet of rubber ($\ell_g \approx 1$ cm) in various geometries. (*b*) A circular sheet of rubber (≈2.5 m) is suspended from one point. (*c*) A sheet of length $L \approx 2.5$ m and its width $W \approx 1$ m is bunched together along a linear clamped boundary so that $\Delta \approx 20$ cm, and the imposed wavelength there is $\lambda_d \approx 5$ cm. The wavelength λ increases as we move away from the clamped boundary as does the characteristic persistence length, L_d. The persistence length for the first generation of wrinkles is $L_d \approx 10$ cm. (*d*) A circular table of radius $R_i \approx 12$ cm is draped symmetrically with a circular sheet of radius $R \approx 52$ cm. The number of folds: $n = 10$. (e) A schematic of the folds in *d* showing the geometry of the sheet and the longitudinal and transverse forces induced by gravity.

Comparing the result with the second expression in Eq. **1** leads to the relations

$$\dot{\beta} = -\sin\phi$$
$$\dot{\theta} = \cos\phi/\sin\beta. \qquad [3]$$

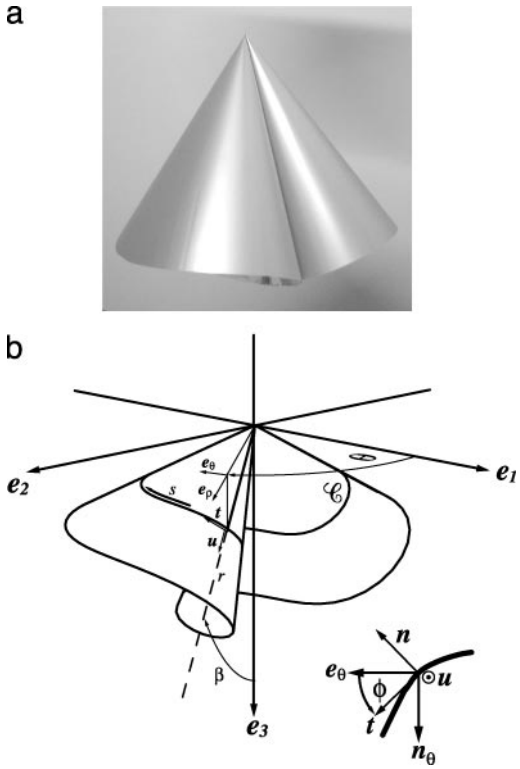

Fig. 2. Simple conical folds. (*a*) The shape of a circular sheet of wrapping paper with $R/\ell_g \approx 6$ suspended from a point shows a single fold. (*b*) The moving coordinate system on the surface **t**,**u**,**n** can be characterized in terms of the three Euler-like angles $\{\theta, \beta, \phi\}(s)$.

In terms of **t**, the tangent to the curve $\mathcal{C}$, and $\mathbf{n} = \mathbf{t} \times \mathbf{u}$, the normal to the surface, the only nonzero surface curvature is $1/R_c = \kappa/r$, where $\kappa = -\mathbf{n}\cdot\dot{\mathbf{t}}$.[f] Differentiating the second expression in Eq. **1** for the curvature then yields

$$\dot{\phi} = \kappa - \cot\beta\cos\phi. \qquad [4]$$

The three relations (**3**, **4**) are the analogous to the Frenet equations for a curve (10) and can be integrated once κ is known to yield the shape of the conical surface. In addition, the azimuthal periodicity of the surface yields $\theta(2\pi) = \theta(0)$ so that integrating the second of the relations in Eq. **3** for the projected polar angle θ yields

$$0 = \int_0^{2\pi} ds(1-\cos\phi/\sin\beta). \qquad [5]$$

We now consider the total energy of the system

$$U = U_B + U_G = \frac{B}{2}\int_A dA\frac{1}{R_c^2} - h\rho g\int_A dAz, \qquad [6]$$

where $B = Eh^3/12(1-\nu^2)$ is the bending stiffness, ν is Poisson's ratio, h is the thickness, ρ is the density, and g is gravity. Inspection of the energy shows that a natural length scale in the problem arises from the balance of gravitational and bending energies, the "gravity length" $\ell_g = (B/h\rho g)^{1/3}$ (11). For the rubber sheet (Fig. 1*b*) $\ell_g \approx 1$ cm, whereas for the wrapping paper

[f]Here, the center of curvature is in the direction of $-\mathbf{n}$ so that $\kappa > 0$ when the shape is a perfect cone.

(Fig. 2*a*) $\ell_g \approx 3$ cm. Integrating Eq. **6** in the radial direction, we find that the gravitational energy $U_G = -\frac{1}{3}h\rho g R^3 \int_0^{2\pi} ds \cos\beta$ and the bending energy $U_B = \frac{1}{2}B\int_A dA\kappa^2/r^2 = \frac{1}{2}B\ln(R/R_*)\int_0^{2\pi} ds\kappa^2$, where R_* is the size of the tip or core, where double curvature and stretching effects cannot be neglected. Then the total dimensionless Lagrangian is[g]

$$L = \frac{1}{2}\int_0^{2\pi} ds\ \kappa^2 + \eta\int_0^{2\pi} ds\ \cos\beta - \lambda\int_0^{2\pi} ds(1 - \cos\phi/\sin\beta). \qquad [7]$$

Here $\eta = (R/\ell_g)^3/3\ln(R/R*)$, and λ is the Lagrange multiplier that enforces the continuity constraint embodied in Eq. **5**. Extremizing the Lagrangian L we get an equation for the curvature

$$\ddot{\kappa} + (a^2 + \kappa^2/2)\kappa = -\eta(\kappa\cos\beta - \sin\beta\cos\phi), \qquad [8]$$

where a^2 is a constant of integration related to the Lagrange parameter λ. It is noteworthy that when $\eta = 0$ Eq. **8** is integrable in terms of elliptic functions. In fact, this is the equation for the planar *Elastica* of Euler (4), i.e., in the absence of gravity, bending a surface into a conical shape is equivalent to the planar bending of an elastic bar even in the large deformation regime associated with geometrically exact kinematics.

Solving Eqs. **3**, **4**, and **8** numerically with periodic boundary conditions, we find that when $\eta < \eta_c$ the solution with the least energy has two folds $n = 2$,[h] with the total energy $\partial U/\partial n > 0$. The numerical procedure, implemented in *Mathematica* (12), starts with the solution to the linearized versions of Eqs. **3**, **4**, and **8**, which serves as a first guess in a homotopy or continuation method that increases the strength of the nonlinearity and/or gravity gradually.[i] When $\eta = \eta_c \approx 5.8$ the solution with two folds exchanges stability with a lower energy solution having only one fold (see Fig. 3), which breaks the symmetry with respect to the plane $\mathbf{e}_1 - \mathbf{e}_3$. Fig. 3*a* shows the shape of both solutions for $\eta \approx 6.1$ when the generator at $s = \pi$ just touches the one at $s = 0$ for the second shape.[j] This behavior of the solution for small sheets is characteristic of rubber but not for wrapping paper. Fig. 4 *a* and *b* shows that two small sheets with $R \approx 4\ell_g$, one of wrapping paper and the other of rubber, have different structures. For small sheets, two solutions are possible: a cylindrical form with parallel generators (Fig. 4*a*) or a conical form with two folds (Fig. 4*b*). The intuitive explanation for this difference arises from considerations of the core bending energy that increases logarithmically with the size of the tip, R_*, so that a surface with a smaller tip but the same value of R/ℓ_g will have a higher energy. We note that although $R_* \sim h^{1/3}R^{2/3}$ (8), here we treat it as a parameter because of its appearance in the argument of a logarithm. For wrapping paper the core size (smaller than that for rubber sheet) can be so small that the cylindrical shape without a singularity is the solution with the lowest energy. Fig. 4*c* shows the energy for the different solutions and two different values of the dimensionless parameter R_*/ℓ_g consistent with our experimental observations. If the sheet is large enough however, the conical shape with one fold (Fig. 2*a*) is always the preferred solution because the extra core bending energy is more than compensated for by the reduction of the gravitational energy caused by a single fold.

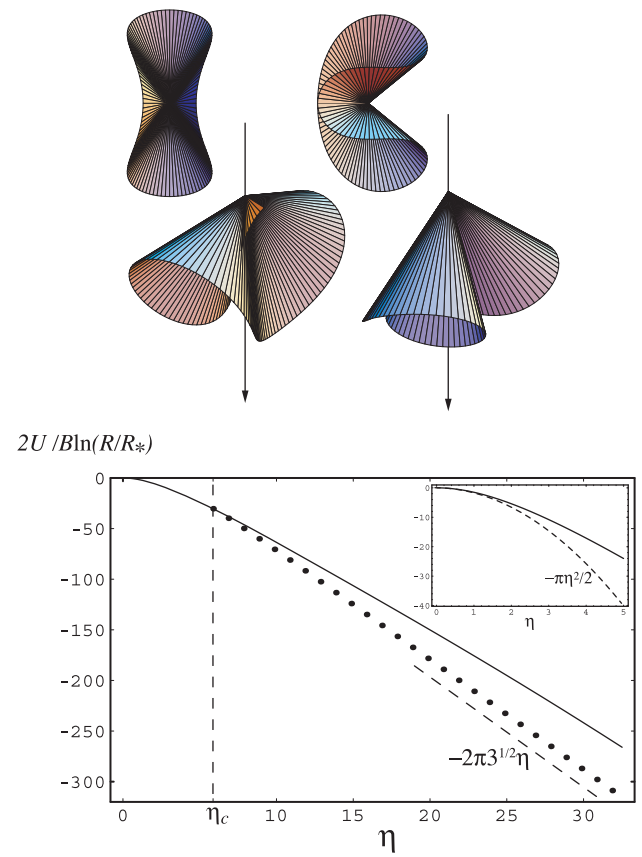

Fig. 3. Bistability in conical folding. (*a*) Different views of the equilibrium shapes obtained for $\eta \approx 6.1 > \eta_c$. (*Left*) A cone with two folds. (*Right*) A cone with one fold. (*b*) Dimensionless total energy $2U/B\ln(R/R_*)$ as a function of η. The solid line corresponds to a conical shape with two folds, and the dotted line corresponds to a cone with one fold. For small sheets with $\eta < \eta_c$ only a cone with two folds exists. For comparison, the dashed line shows the energy of a big sheet with constant opening angle $\beta = \pi/6$ made by folding a semicircle of the same material. (*Inset*) The energy following a linear analysis of Eq. **7** matches the numerical solution for $\eta < 2$.

Scaling Laws for Complex Folds

When the sheet radius $R/\ell_g \gg 1$, a large number of folds is the result; however, the lack of any symmetry along with the problem of self-contact of the folds makes an exact analysis difficult. Therefore, we use scaling arguments to tease out the general trends of the solution. The gravitational energy can be minimized by reducing the azimuthal deflection angle β, but this process increases the number of folds (because of the inextensibility condition) and hence the bending cost, so that the result is an optimal number of folds minimizing the total energy. When the folds are large in number and nearly vertical, $\theta \approx \pi/2$, $\beta \ll 1$ and the kinematic equations (**3** and **4**) yield $\ddot{\beta} \approx \kappa$. Then $U_B \sim B\ln(R/R_*)\ddot{\beta}^2$ and $U_G \sim h\rho g R^3\beta^2 + cst$ and their sum is a minimum when $U_B \sim U_G$. Using $\dot{\beta} \sim \beta/\delta s$ in the previous relation leads to the characteristic arc length of a single fold $\delta s \sim 1/\eta^{1/4}$ and the number of folds n is given by

$$n = \frac{2\pi}{\delta s} \sim \frac{(R/\ell_g)^{3/4}}{\ln(R/R_*)^{1/4}} \qquad [9]$$

an increasing function of the system size R.

[g] We should also include the condition for global torque balance. Equivalently, $\vec{g} \times \vec{R}_{CM} = 0$, where $\vec{R}_{CM}$ is the center of mass. Here, the solutions of Eq. **7** identically satisfy the balance for torques.

[h] Our definition of the number of folds is formally given by the number of times the curvature changes sign as s varies from $s = 0$ to $s = 2\pi$.

[i] Solving the linearized equations yields n-fluted conical shapes, of which the two-fluted solution has the minimum energy. However, for large sizes of the "core" region R_* where the developable solution fails, the cylindrically deformed shape can have an even lower energy and is preferred.

[j] The generator at $s = 0$ is chosen as the point with maximal negative curvature.

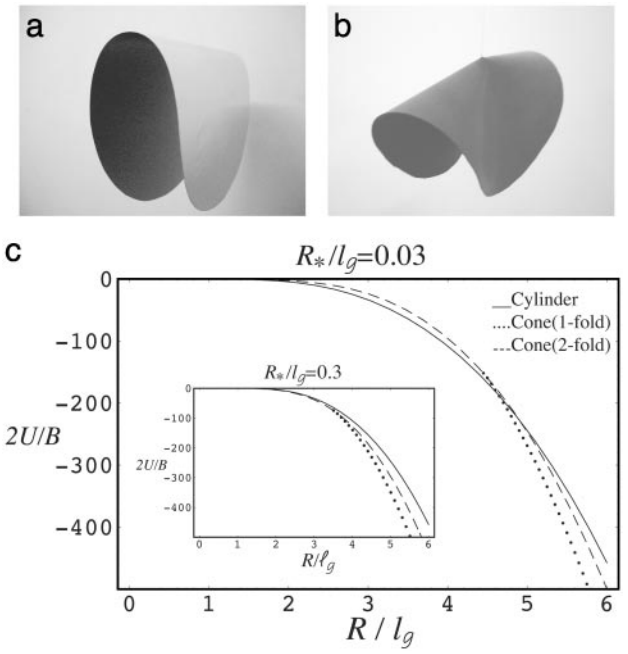

Fig. 4. Transitions between different draping configurations. (*a*) A small circular sheet of wrapping paper with radius $R \approx 4\ell_g$ deforms into a cylindrical surface. (*b*) On the other hand, a circular sheet of rubber with radius $R \approx 4\ell_g$ but with a thickness 50 times that of wrapping paper deforms into a cone. (*c*) The dimensionless total energy for different solutions. To allow for comparisons with a cylindrical shape, we use $2U/B$, instead of $2U/B\ln(R/R_*)$ and the parameter R/ℓ_g instead of η. For wrapping paper $R_* \approx 1$ mm and $R_*/\ell_g \approx 0.03$, the minimal energy solution is cylindrical when $R/\ell_g \lesssim 5$ and a conical when $R/\ell_g \gtrsim 5$. (*Inset*) If $R_*/\ell_g = 0.3$, i.e., the core size is large, the conical shape is energetically favorable for all R/ℓ_g.

We now expand our arguments to include stretching effects and different geometries for the suspension frames. Consider the draping of a circular table of radius $R_i < R$, a test used by the textile industry to quantify the "hand" (13) or the ability to drape a body (Fig. 1*d*). Since the typical fold wavelength is much smaller than the radius of the table for a heavy sheet, a Cartesian description is sufficient to describe the problem, with $x \in [0, L]$, $L = R - R_i$, being the distance from the edge of the table, y the azimuthal coordinate, $T = h\zeta g(L-x)$, the force due to gravity on the sheet at a vertical distance x from the point of suspension, and ζ the deviation from a right cylinder of radius R_i (Fig. 1*e*). The minimum gravitational potential energy state $\zeta = 0$ cannot be achieved since the cost of bending the tablecloth is not small. Indeed the bending energy $U_B = \frac{1}{2}\int_A B(\partial_y^2\zeta)^2 dA$ makes it transparent that the total energy increases rapidly for short wavelengths. On the other hand, both the longitudinal component $T\cos\beta \sim T \sim \rho g h L$, which stretches the surface and the transverse component $T\sin\beta \sim T\beta$ cause the tablecloth to become vertical (Fig. 1*e*) as follows. The combination of the longitudinal curvature of the sheet $\partial_x^2\zeta \sim \zeta/L^2$ and the longitudinal tension leads to an out-of-plane pressure $T\partial_x^2\zeta \sim T\zeta/L^2$, which tends to favor gravity and lower the sheet. Similarly the transverse component of the force leads to an out-of-plane pressure $T\beta/L \sim T\zeta/L^2$ with the same effect. These additional forces (per unit area) can be derived from the energy of an "effective" elastic foundation (14) supporting a thin sheet $U_F = \frac{1}{2}\int_A K\zeta^2 dA$, where $K \sim T/L^2 \sim h\rho g/L$ is the stiffness of the foundation. Comparing the bending and stretching (gravitational) energies, we see that the optimal wavelength scales as $\lambda \sim (B/K)^{1/4} \sim \ell_g^{3/4}L^{1/4}$. Because the number of folds n does not change from the edge of the table to the end of the tablecloth of Fig. 1*d*, we conclude that $\lambda/R \approx \lambda_i/R_i$, λ_i being the wavelength at the edge of the table. Therefore, $n = 2\pi R_i/\lambda_i \sim R/(\ell_g^3 L)^{1/4}$. When $R \sim L \gg R_i$, $n \sim (R/\ell_g)^{3/4}$, corresponding to the result obtained in Eq. **8**. For the circular table in Fig. 1*d*, $L \approx 40$ cm, $R_i \approx 12$ cm $< L$, and $\ell_g \approx 1$ cm, so that $n \approx 15$, consistent with the observations where $n = 10$.

We finally turn to the case when a sheet is suspended along a line (Fig. 1*c*). In typical drapes and curtains, for aesthetic reasons, the sheet is forced to bunch up to form a series of short wavelength folds as its lateral ends are brought together by a distance Δ along the line of suspension. Away from the line, these folds coalesce into larger and larger folds. This inverse cascading of length scales can be understood in terms of the persistence length L_d of a wrinkle in a stretched strip, defined as the distance over which a sheet pinched at one end with an amplitude ζ and width λ_d eventually flattens out. Balancing the stretching and bending energies over the length L_d, yields $U_B \sim B(L_d\lambda_d)\zeta^2/\lambda_d^4 \sim U_S \sim T(L_d\lambda_d)\zeta^2/L_d^2$ so that $L_d \sim \lambda_d^2(T/B)^{1/2}$. Comparing this with the persistence length L for a fold of natural wavelength yields $L_d/L \sim (\lambda_d/\lambda)^2$; for the drape (Fig. 1*c*), $L \approx 250$ cm, $\lambda_d \approx 5$ cm, and $\lambda \approx 25$ cm, so that $L_d \approx 10$ cm, consistent with observations. This persistence effect might also explain the periodically placed horizontal guy ropes in wrapped buildings (3), which serve to accentuate the shape of the draped object while preserving the aesthetics of the wrinkles. Seen differently, the natural wavelength in this system is again $\lambda \sim \ell_g^{3/4}L^{1/4}$, so that the number of folds along the width W of the sheet is $n = W/\lambda \sim L^{-1/4}$ (corresponding to the case $L \ll R_i$ for the circular table), decreases with system size, in marked contrast with the result for a circular table, and consistent with observations.

Discussion

In conclusion, we have used a combination of analytical and scaling arguments to quantify the basic components of a complex drapery as a function of system size and the boundary conditions (geometry of suspension). Our approach bridges the gap between simple cantilever analyses of cylindrical deformations (9, 12) and large-scale computation (6, 7), by focusing on those aspects of the problem amenable to an approximate analysis. Even restricting ourselves to simple geometries, we find that qualitatively different shapes of the drapery may be separated by relatively small energetic barriers. Thus it is easy to have dynamic transitions between states. Indeed in fashion design and on catwalks, this is precisely what gives rise to the aesthetic appearance of a kinetic sculpture in motion. The inherent metastability that we have uncovered even in the simplest of drapes shows that previous purely computational approaches to fabric design could be usefully complemented by qualitative approaches before we can unravel the complexities of and transitions between multistable patterns.

To go beyond the elements and piece them together to complete the whole, we have to "stitch" the resulting cones, cylinders, and flat sheets together much as a couturier does, using boundary layers, narrow regions with relatively rapid variations where one solution merges into another and where the sheet will be both bent and stretched. The location of these regions is determined by the requirement of energy minimization (subject to the constraints of draping the rigid object). However, the energy stored in the boundary layers is negligible compared with the total energy (8), which is predominantly stored in isometric bending. Then, it is possible to refine the solution to account for such effects as finite stretching in the regions of double curvature, the effects of textile anisotropy, and other higher-order effects.

We thank Jacques Dumais for help with photography. E.C. acknowledges the support of a Fundación Andes postdoctoral fellowship (2001), Universidad de Santiago Departamento de Investigación Científicas y

Tecnológica project "The tablecloth problem" (1999–2001), Fondo Nacional de Investigacion Científica y Tecnologica Grant 1020359 (2002), and Fondo de Investigación Avanzada en Áreas Prioritarias Grant 11980002 (2002). L.M. acknowledges the support of the Schlumberger Chair Fund, the National Institutes of Health, and the U.S. Office of Naval Research.

1. da Vinci, L. (1983) *Drawings* (Dover, Mineola, NY).
2. Constantine, M. & Reuter, L. (1997) *Whole Cloth* (Monacelli, New York).
3. Christo, Volz, W. & Bourdon, D. (1996) *Wrapped Reichstag, Berlin, 1971–1995* (Taschen, Los Angeles).
4. Landau, L. & Lifshitz, E. M. (1986) *Theory of Elasticity* (Pergamon, New York), 3rd Ed.
5. Antman, S. S. (1993) *Nonlinear Problems of Elasticity* (Springer, New York).
6. Van West, B. P., Pipes, R. B. & Keefe, M. (1990) *J. Textile Inst.* **81,** 448–460.
7. Chen, B. & Govindaraj, M. (1995) *Textile Res. J.* **65,** 324–330.
8. Cerda, E., Chaieb, S., Melo, F. & Mahadevan, L. (1999) *Nature*, **401,** 46–49.
9. Hearle, J. W. S. & Amirbayat, J. (1996) in *The Mathematics of Deforming Surfaces*, eds. Dritschel, D. & Perkins, R. J. (Oxford Univ. Press, London), pp. 33–57.
10. Struik, J. D. (1988) *Lectures on Classical Differential Geometry* (Dover, Mineola, NY).
11. Mahadevan, L. & Keller, J. B. (1995) *SIAM J. Appl. Math.* **55,** 1609–1624.
12. Wolfram, S. (2003) *The Mathematica Book* (Wolfram, Champaign, IL).
13. Hearle, J. W. S., Grosberg, P. & Backer, S. (1969) *Structural Mechanics of Fibers, Yarns, and Fabrics* (Wiley, New York).
14. Cerda, E. & Mahadevan, L. (2003) *Phys. Rev. Lett.* **90,** 74302.